scientific reports

Check for updates

OPEN

Compellingly high SARS-CoV-2 susceptibility of Golden Syrian hamsters suggests multiple zoonotic infections of pet hamsters during the COVID-19 pandemic

Claudia Blaurock[1], Angele Breithaupt[2], Saskia Weber[1], Claudia Wylezich[3], Markus Keller[1], Björn-Patrick Mohl[1], Dirk Görlich[4], Martin H. Groschup[1], Balal Sadeghi[1], Dirk Höper[3], Thomas C. Mettenleiter[5] & Anne Balkema-Buschmann[1]✉

Golden Syrian hamsters (*Mesocricetus auratus*) are used as a research model for severe acute respiratory syndrome coronavirus type 2 (SARS-CoV-2). Millions of Golden Syrian hamsters are also kept as pets in close contact to humans. To determine the minimum infective dose (MID) for assessing the zoonotic transmission risk, and to define the optimal infection dose for experimental studies, we orotracheally inoculated hamsters with SARS-CoV-2 doses from $1 * 10^5$ to $1 * 10^{-4}$ tissue culture infectious dose 50 ($TCID_{50}$). Body weight and virus shedding were monitored daily. $1 * 10^{-3}$ $TCID_{50}$ was defined as the MID, and this was still sufficient to induce virus shedding at levels up to $10^{2.75}$ $TCID_{50}$/ml, equaling the estimated MID for humans. Virological and histological data revealed $1 * 10^2$ $TCID_{50}$ as the optimal dose for experimental infections. This compelling high susceptibility leading to productive infections in Golden Syrian hamsters must be considered as a potential source of SARS-CoV-2 infection for humans that come into close contact with pet hamsters.

To date, more than 528 million confirmed Coronavirus Disease 2019 (COVID-19) cases and more than 6.2 million deaths have been reported globally since the initial detection of severe acute respiratory syndrome coronavirus 2 (SARS-CoV-2) in December 2019 (https://coronavirus.jhu.edu; 28th May 2022). COVID-19 has been studied extensively since, and the incubation time in humans has been calculated as 6.4 days for the initially described virus variants[1,2], while the estimated minimum infective dose (MID) for humans has been calculated to be approximately 10^2 tissue culture infectious dose 50 ($TCID_{50}$)[3,4].

Golden Syrian hamsters (*Mesocricetus auratus*) are widely used as a COVID-19 animal model, as they efficiently support SARS-CoV-2 replication and display pathological manifestations similar to human COVID-19 pneumonia, such as focal diffuse alveolar destruction, hyaline membrane formation, and mononuclear cell infiltration[5,6]. Efficient transmission from inoculated to naïve hamsters by direct contact and aerosol has also been reported[6,7]. Several hamster species are kept as pets in millions of households worldwide. These include Golden Syrian hamsters, Chinese hamsters (*Cricetulus griseus*), and three Dwarf hamster species (*Phodopus roborowskii*, *P. campbelli* and *P. sungorus*). According to the German Pet Trade & Industry Association (Zentralverband Zoologischer Fachbetriebe e.V. ZZF), approximately 520,000 pet hamsters were kept in German households in 2020. Golden Syrian hamsters comprised 43% (223,600 animals), and the Dwarf hamster species 54% (280,800 animals) (source: Zentralverband Zoologischer Fachbetriebe (ZZF) and Industrieverband Heimtierbedarf (IVH)). While Golden Syrian hamsters, Chinese hamsters, and Roborovski Dwarf hamsters are highly susceptible and develop clinical disease and lung pathology, both other Dwarf hamster species (Campbell's Dwarf hamster and

[1]Institute of Novel and Emerging Infectious Diseases, Friedrich-Loeffler-Institut, Greifswald-Insel Riems, Germany. [2]Department of Experimental Animal Facilities and Biorisk Management, Friedrich-Loeffler- Institut, Greifswald-Insel Riems, Germany. [3]Institute of Diagnostic Virology, Friedrich-Loeff ler-Institut, Greifswald-Insel Riems, Germany. [4]Max Planck Institute for Multidisciplinary Sciences, Göttingen, Germany. [5]Friedrich-Loeffler-Institut, Federal Research Institute for Animal Health, Greifswald-Insel Riems, Germany. ✉email: anne.buschmann@fli.de

Djungarian Dwarf hamster) only developed subclinical disease with mild tissue damage and a rapid onset of regeneration under experimental conditions[8,9].

Since the onset of the pandemic, several virus variants have emerged, five of which have been classified as variants of concern (VOC) by the World Health Organization (WHO) for their enhanced transmissibility and virulence or their reduced susceptibility to immune reactions (WHO, 01.03.2022). These include variants B.1.1.7 (Alpha), B.1.351 (Beta), P.1 (Gamma), B.1.617.2 (Delta) and B.1.1.529 (Omicron). Especially the rapid worldwide spread of the Delta variant and a number of Omicron subvariants have raised concern about an acceleration of the pandemic's dynamic, despite increasing proportions of fully vaccinated humans (https://github.com/owid/covid-19-data/tree/master/public/data/vaccinations). Therefore, the pathogenesis induced by VOCs has been addressed in a number of recent animal studies, mostly performed in Golden Syrian hamsters[10–13]. While Alpha, Beta and Delta variants caused clinical manifestation and pathology similar to the ancestral virus[10,11], infection with the Omicron variant BA.1 caused significantly milder clinical signs and lower levels of pulmonary affection[12,13]. The reported levels of viral RNA detected in the respiratory tract of these animals however vary between the available study reports, and may therefore need further confirmation[12–14].

Very recently, two distinct zoonotic transmission events from hamsters to humans were reported from Hong Kong followed by human-to-human transmission[15], after the import of pet Golden Syrian hamsters from The Netherlands, causing a re-introduction of the Delta VOC into the country. Investigation of these animals revealed SARS-CoV-2 RNA in 15 out of 28 Golden Syrian hamsters, but in none of the 77 analysed Dwarf hamsters[15]. These findings gave rise to serious concern about the SARS-CoV-2 transmission risk from pet hamsters to humans in affected households[16,17], and more than 2000 pet hamsters were subsequently culled in Hong Kong. This highlights the importance of an evidence-based risk assessment regarding SARS-CoV-2 transmissions from pet hamsters to humans and vice versa. To the best of our knowledge, no systematic quantitative study on the susceptibility of Golden Syrian hamsters to a SARS-CoV-2 infection has been undertaken so far. We therefore infected groups of Golden Syrian hamsters with serial SARS-CoV-2 dilutions from 10^5 to 10^{-4} $TCID_{50}$, which is equivalent to 0.7 genome copy numbers per dose, as determined by reverse transcriptase quantitative real-time PCR of serial dilutions of a SARS-CoV-2 RNA standard. Animals infected with a dose of $1 * 10^{-3}$ $TCID_{50}$ shed replication competent virus and accumulated SARS-CoV-2 infectivity in their respiratory tract until 7 days post inoculation (dpi). This study demonstrates the extremely high SARS-CoV-2 susceptibility of Golden Syrian hamsters. For drug or vaccine efficacy studies, a moderate infection dose, sufficiently high to induce reproducible viral loads and histological findings, and at the same time sufficiently low to avoid a highly artificial infection should be applied, which in our experimental setup was determined as $1 * 10^2$ $TCID_{50}$.

Methods

Experimental design. This study was performed to quantify the susceptibility of Golden Syrian hamsters to an infection with SARS-CoV-2. All SARS-CoV-2 experimental studies were performed in the biosafety level 3 facilities at the Friedrich-Loeffler-Institut, Insel Riems, Germany.

Cell line and virus. Vero E6 cells (Cell Culture Collection in Veterinary Medicine, FLI) were cultured in minimal essential medium (MEM) containing 10% fetal calf serum (FCS) at 37 °C and 5% CO_2. SARS-CoV-2 isolate 2019_nCoV Muc-IMB-1 (accession number LR824570;[18]) was kindly provided by Bundeswehr Institute of Microbiology, Munich, Germany. Virus propagation was maintained in Vero E6 cells in DMEM supplemented with 2% FCS. Prior to inoculation into hamsters, the virus stock was sequenced by using a generic metagenomics sequencing workflow as described previously[19] with some modifications. For reverse-transcribing RNA into cDNA, SuperScriptIV First-Strand cDNA Synthesis System (Invitrogen, Germany) and the NEBNext Ultra II Non-Directional RNA Second Strand Synthesis Module (New England Biolabs, Germany) were used, and library quantification was done with the QIAseq Library Quant Assay Kit (Qiagen, Germany). Libraries were sequenced without applying further SARS-CoV-2 enrichment using an Ion 530 chip and chemistry for 400 base pair reads on an Ion Torrent S5XL instrument (Thermo Fisher Scientific, Germany).

Virus titration: tissue culture infectious dose$_{50}$. Samples were serially diluted in MEM containing 2% FCS and 100 Units Penicillin/0.1 mg Streptomycin (P/S) (Millipore Sigma, Germany). Vero E6 cells were incubated with 100 µl of ten-fold dilutions of sample dilutions added in quadruplicates for 1 h at 37 °C before 100 µl MEM containing 2% FCS and P/S were added per well and plates were incubated for 5 days at 37 °C and 5% CO_2. Supernatant was removed and cells were fixed with 4% formalin. Next, plates were stained with 1% crystal violet and titers were determined following the Spearman Kaerber method[20].

Animal studies. Male Golden Syrian hamsters (*Mesocricetus auratus*), 5–7 weeks old with a body weight of 80–100 g, were obtained from Janvier Labs, France. Three hamsters were housed in individually ventilated cages (IVC). Animals had ad libitum access to food and water. The animals' well-being and body weight were checked daily. Handling and sampling were performed starting with the uninfected group and continuing from the low dose groups to the high dose groups to minimize the contamination risk.

Inoculation routes. To determine the optimal inoculation route for SARS-CoV-2, we inoculated groups of eight hamsters under isoflurane anaesthesia in parallel by the intranasal and orotracheal route with 100 µl containing $1 * 10^5$ $TCID_{50}$. For the orotracheal challenge, the inoculum was administered on the root of the tongue, ensuring aspiration of the inoculum with the following inhalation. Oral swab samples were collected in DMEM containing P/S daily, starting one day before inoculation (− 1 dpi). Nasal washes were collected under isoflurane anaesthesia at days 2, 4, 6, 9, 11 and 13 by flushing 200 µl PBS along the animal's nose. At 14 dpi, hamsters were

euthanized by deep isoflurane anaesthesia, cardiac exsanguination and cervical dislocation, and nasal conchae, trachea and lung samples were collected and stored at – 80 °C for virological analysis. Tissue samples were also stored in 4% neutral-buffered formalin for histopathological analysis. Serum was separated from the collected blood.

Titration in hamsters. To define the MID, three sets of experiments were performed, as the endpoint in the first two studies was not reached. For animal welfare reasons, we continued the dilutions in the second and third experiment, including an overlap ensuring the comparability of results.

First, hamsters were inoculated with a dose of $1 * 10^5$ $TCID_{50}$ SARS-CoV-2 and with serial dilutions from $1 * 10^3$ to $1 * 10^{-1}$ $TCID_{50}$ (n = 3 per dilution; total n = 21). Oral swab samples were collected at 1, 3, 5, and 6 dpi, nasal washes were collected at 2 and 4 dpi as described above). At 7 dpi, all hamsters were euthanized and sampled as described above.

In the second study, hamsters were inoculated with a serial dilution from $1 * 10^4$ to $1 * 10^{-3}$ $TCID_{50}$ SARS-CoV-2 (n = 3 per dilution; total n = 28). Group sizes of three hamsters per dilution were set based on statistical requirements. All animals were included in the analysis. Sampling and autopsies were performed as described above.

In the third study, hamsters were inoculated with $1 * 10^2$ $TCID_{50}$, and with serial dilutions from $1 * 10^0$ to $1 * 10^{-4}$ $TCID_{50}$ SARS-CoV-2 (n = 3 per dilution; total n = 21). This experiment was conducted for 10 days to allow the follow-up of clinical and virological data after a 2–3 day delayed disease onset in the groups inoculated with low doses. Oral swab samples were collected at 1, 3, 5, 6, 8 and 9 dpi, while nasal washes were collected at 2, 4 and 7 dpi. At 10 dpi, animals were sacrificed and autopsied as described above.

Ethical statement. Ethical approval for this study was obtained from the competent authority of the Federal State of Mecklenburg-Western Pomerania, Germany upon consultation with the Ethic Committee of Mecklenburg-Western Pomerania (file number: 7221.3-1.1-049/20), on the basis of national and European legislation, namely the EU council directive 2010/63/EU. Animal studies are continuously monitored by the Animal Welfare Officer and were approved by FLI's Institutional Animal Care and Use Committee (IACUC). All procedures and methods for the animal study were performed in accordance with the relevant national and international guidelines and regulations. The study is reported in accordance with ARRIVE guidelines.

Total RNA extraction and SARS-CoV-2 detection. Total RNA was extracted from swab, nose fluid and tissue samples as described earlier[21]. SARS-CoV-2 RNA was detected using "Envelope (E)-gene Sarbeco 6-carboxyfluorescein quantitative RT-PCR"[22] as described previously[21]. Viral genome copy numbers were calculated from standard curves determined for 10^{-2} to 10^{-5} dilutions containing known copy numbers of SARS-CoV-2.

Selected samples were analysed for the presence of subgenomic RNA (sgRNA) as an indication of virus replication, using a published protocol[23,24]. Quantitative Realtime PCR was performed with the qScript XLT One-Step RT-qPCR ToughMix (QuantaBio/VWR). Primer sequences for the ORF 7a detection are available upon request.

Indirect SARS-CoV-2 RBD ELISA. SARS-CoV-2 specific antibodies were detected using a published protocol[25] with the modification of using a 1:30,000 dilution of Protein A/G (Thermo Fisher) in exchange of the multi-species conjugate.

To determine a cut-off-value and the diagnostic sensitivity of this modified assay, we tested 53 negative hamster sera and 227 sera of SARS-CoV-2 infected hamsters. The area under the receiver operating characteristic (ROC) curve was used to determine the ELISA cut-off-value. Statistical analyses were performed using MedCalc for Windows, version 19.4 (MedCalc Software, Ostend, Belgium). p-value < 0.01 was regarded as statistically significant.

Lateral flow device (LFD) rapid test. Oral swab samples of groups inoculated with $1 * 10^3$ to $1 * 10^{-2}$ $TCID_{50}$ SARS-CoV-2 were collected at 6 dpi in lysis buffer supplied with the Nowcheck COVID-19 LFD (concile GmbH, Freiburg, Germany) testkit. 120 µl of the suspension was applied on the LFD and incubated at RT for 15 min. We also analysed nasal wash samples collected at 7 dpi by diluting 25 µl of the fluid into 300 µl of the supplied lysis buffer and applying 120 µl of this mixture to the LFD. Evaluation of the control (C) and test (T) bands was performed according to the instructions. LFDs were imaged and densitometry was performed on the C and T bands using ImageJ (ImageJ 1.52a, Wayne Rasband, NIH, USA). These band quantifications were used to calculate a T/C ratio. Standard deviation was calculated from the T/C ratios within each respective group.

Pathology of lung samples collected at 10 dpi. During autopsy, the lung surface was evaluated and the percentage of macroscopically detectable areas of consolidation (dark red discoloration) per total lung tissue was estimated by trained veterinarians. The left lung lobe was carefully removed, immersion-fixed in 10% neutral-buffered formalin, paraffin-embedded, and 2–3-µm sections were stained with hematoxylin and eosin (HE). Slides were scanned using a Hamamatsu S60 scanner, and evaluated using the NDPview.2 plus software (Version 2.8.24, Hamamatsu Photonics, K.K. Japan). The lung tissue was evaluated using a 500 × 500 µm grid, and the extent of pneumonia-associated consolidation was recorded as percentage of affected lung fields. Further, the lung was examined for the presence of SARS-CoV-2-characteristic lesions described for hamsters, i.e. intra-alveolar, interstitial, peribronchial and perivascular inflammatory infiltrates, alveolar edema, necrosis of the bronchial and alveolar epithelium, diffuse alveolar damage, vasculitis or endothelialitis, pneumocyte type 2

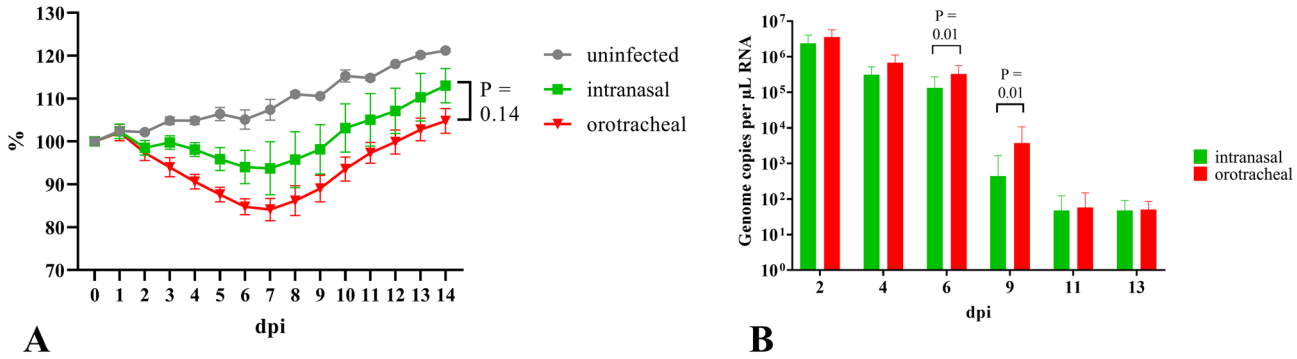

Figure 1. Orotracheal SARS-CoV-2 inoculation results in increased weight loss and viral shedding. (**A**) Body weight curves of uninfected control group (grey), groups infected by the nasal (green) and orotracheal (red) routes; (**B**) Nasal shedding between 1 and 13 dpi after intranasal (green) and orotracheal (red) inoculation.

hyperplasia/hypertrophy with bronchialisation and atypical cells, and hypertrophy/hyperplasia of the bronchial epithelium. Archived lung tissues from hamsters infected with $1 * 10^{4.5}$ $TCID_{50}$ were included as positive controls. Evaluation and interpretation were performed by a board-certified pathologist (DiplECVP) following a post examination masking approach[26].

Sequence analysis. Full genome sequences were generated via reference mapping with the Genome Sequencer software suite (version 2.6; Roche; default software settings for quality filtering and mapping), using SARS-CoV-2 strain 2019_nCoV_Muc_IMB1 (accession number LR824570) as reference. Consensus sequences and underlying sequence reads were visualized using Geneious Prime (10.2.3; Biomatters, Auckland, New Zealand). The presence of single nucleotide variants (SNVs) was checked using the variant analysis tool implemented in Geneious Prime (default settings, minimum variant frequency 0.02).

Statistical analysis. Mean values determined for the experimental groups were compared using analysis of variance (ANOVA) with Tukey's post-hoc tests for multiple comparisons and non-parametric Kruskal–Wallis test followed by the Dunn's method for multiple comparisons. Data were analyzed using GraphPad Prism (version 9; GraphPad Software, Inc., CA, USA) and SPSS software (IBM Corp. Released 2011. IBM SPSS Statistics for Windows, Version 20.0, IBM Corporation, Armonk, NY, USA). *P*-value < 0.05 was considered statistically significant. Details on statistical analyses are summarized in Supplementary Table S1.

For histopathology, data were tested for Gaussian distribution using the Shapiro–Wilk test, followed by one-way ANOVA with Tukey's post-hoc tests for multiple comparison.

Results

Pronounced weight loss and high levels of viral shedding upon orotracheal inoculation. Upon orotracheal and intranasal inoculation (n = 8 per group) with SARS-CoV-2, animals started losing body weight from 2 dpi, and the mean weight loss at 7 dpi was 16% after orotracheal inoculation and 7% after intranasal inoculation (Fig. 1A). We observed a statistically significant five- to tenfold increase in viral genome shedding in the nasal wash samples at 6 and 9 dpi after orotracheal inoculation as compared to the intranasal inoculation (Fig. 1B). Upon necropsy at 14 dpi, viral RNA in the respiratory tract samples was not detectable at levels allowing a quantitative comparison, and no replication competent virus was detected. Based on these data, we decided to continue with the orotracheal inoculation for subsequent experiments.

$1 * 10^{-1}$ $TCID_{50}$ SARS-CoV-2 is sufficient to induce body weight reduction and pneumonia. Animals inoculated in our first study with doses exceeding $1 * 10^{2}$ $TCID_{50}$ SARS-CoV-2 showed a decrease in body weight from 2 dpi, while hamsters inoculated with $1 * 10^{1}$ $TCID_{50}$ gained weight until 5 dpi, before losing weight until the end of the experiment. Animals inoculated with $1 * 10^{-1}$ and $1 * 10^{0}$ $TCID_{50}$ as well as the uninfected controls continued to gain weight throughout the experiment. In the second study, all groups receiving $1 * 10^{-1}$ $TCID_{50}$ or higher lost weight until the end of the experiment, with an onset delayed by 2–3 days in animals infected with $1 * 10^{1}$ and $1 * 10^{0}$ $TCID_{50}$. In a third study, using dilutions to $1 * 10^{-4}$ $TCID_{50}$ and continuing until 10 dpi, doses of 10^{-1} $TCID_{50}$ or higher induced weight loss. Figure 2 summarizes the cumulative body weight data from all three studies of groups infected with doses between $1 * 10^{5}$ and $10 * 10^{-4}$ $TCID_{50}$. Statistical analysis revealed significant differences between the body weights determined per group at the day of the necropsy, i.e. 7 and 10 dpi (Table S1).

During autopsy performed at 7 or 10 dpi, the percentage of lesion-affected lung tissue was recorded. Macroscopically, we observed decreasing estimated levels of lung affection correlated with decreasing infection doses. We still noted areas of consolidation at 7 dpi in animals that had been infected with $1 * 10^{-3}$ $TCID_{50}$ (Fig. 3A). At 10 dpi, even hamsters inoculated with the lowest dose of $1 * 10^{-4}$ $TCID_{50}$ showed lung changes (Fig. 3B).

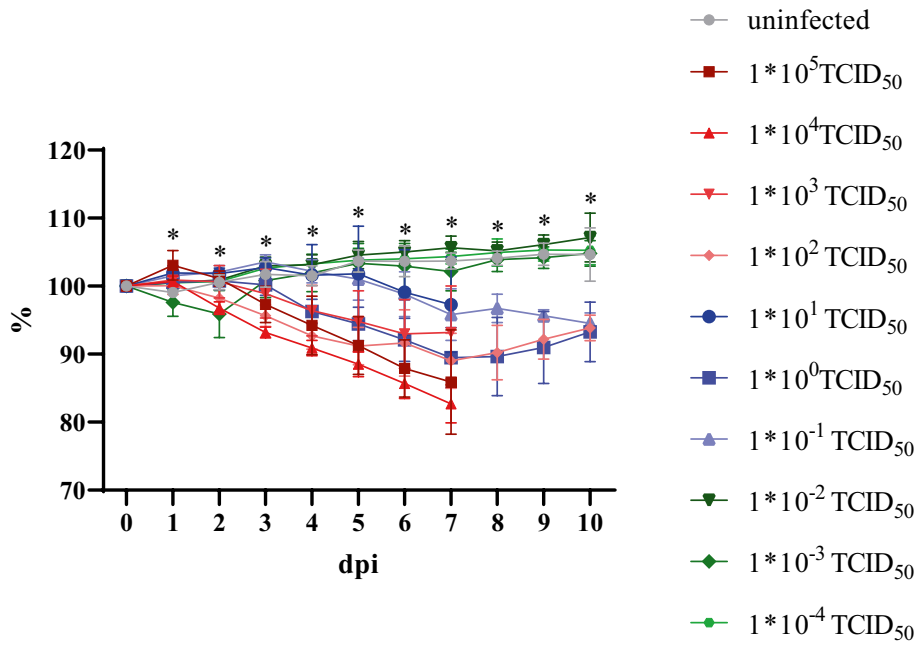

Figure 2. Cumulative mean and standard deviation of three experiments of body weight per infection dose groups. Changes in body weight (%) in relation to 0 dpi. Statistically significant differences in daily body weight changes are marked by an asterisk. $P = 0.0001$ for all days. Further details on statistical analysis are shown in Table S1.

Histopathology was performed on the left lung lobe of animals sacrificed at 10 dpi. Archived lungs from a high-dose infection study ($1 * 10^{4.5}$ $TCID_{50}$) served as positive controls. Pneumonia-associated consolidation was consistently found in all hamsters infected with $1 * 10^{-1}$ $TCID_{50}$ SARS-CoV-2 or higher (Fig. 3C,D).

Lungs collected at 10 dpi mainly showed regenerative changes with bronchial and type-2-pneumoncyte hyperplasia and hypertrophy with formation of multinucleated, atypical cells. However, still a moderate to severe inflammatory reaction was found, with intra-alveolar, interstitial, peribronchial and perivascular inflammatory infiltrates, as well as vasculitis and/or endothelialitis. Acute necrosis of the bronchial epithelium was a rare finding (Fig. 4A–D). Although not statistically significant, hamsters infected with $1 * 10^{-1}$ $TCID_{50}$ showed a tendency to be less severely affected (Fig. 4E). In general, animals infected with doses of $1 * 10^{-2}$ $TCID_{50}$ and lower did not develop pneumonia-associated consolidation in the lung (Fig. 4F,G). However, focal alveolar or perivascular infiltrates or bronchial epithelial hyperplasia were found in individual animals in each group indicating prior local infection, even after infection with $1 * 10^{-4}$ $TCID_{50}$ (Fig. 4H,I).

Lateral flow device rapid test detects infections with $1 * 10^{-1}$ $TCID_{50}$ SARS-CoV-2. We analysed oral swab samples collected 6 dpi using the Nowcheck COVID-19 Rapid Test, which confirmed the infection in hamsters inoculated with doses higher than $1 * 10^{0}$ $TCID_{50,}$ as well as in two hamsters inoculated with $1 * 10^{-1}$ $TCID_{50}$, which translates into samples with ct-values in the real-time RT-PCR below 30. All uninfected control hamsters as well as one hamster inoculated with $1 * 10^{-1}$ $TCID_{50}$ were negative at 6 dpi (Fig. S1). We also analysed nasal washes collected at 7 dpi. Again, the infection was detectable in animals challenged with doses of $1 * 10^{-1}$ $TCID_{50}$ or higher, i.e. for samples with ct-values below 30.

$1 * 10^{-2}$ $TCID_{50}$ SARS-CoV-2 is sufficient to induce seroconversion. To confirm a systemic infection, all sera collected during necropsies were tested in an indirect ELISA based on the SARS-CoV-2 RBD antigen. Receiver operating characteristic (ROC) analysis was performed for the determination of the ELISA cut-off value. We determined a specificity of 100% and a sensitivity of 99.56% using the cut-off value of 14.11 percent of the positive control value (PP) (Fig. S2A). We detected seroconversion with a dose-dependent increase of PP values in hamsters inoculated with infection doses of $1 * 10^{-2}$ $TCID_{50}$ or higher (Fig. S2B).

$1 * 10^{-3}$ $TCID_{50}$ SARS-CoV-2 is sufficient to induce oral and nasal viral shedding. From the first day post infection, animals infected with 10^{2} $TCID_{50}$ SARS-CoV-2 or higher shed virus between $10^{3.5}$ and $10^{4.5}$ genome copy numbers/µl RNA. By 3 dpi, all animals infected with doses of $1 * 10^{-1}$ $TCID_{50}$ or higher shed virus (Fig. 5A). The oral swab samples contained replicating virus even in the groups infected with a dose of 10^{-1} $TCID_{50}$ until 6 dpi, and at a level of 10^{2} $TCID_{50}$/ml in the swab sample collected at 6 dpi from one animal infected with the $1 * 10^{-3}$ $TCID_{50}$ dose. This result was confirmed by the detection of SARS-CoV-2 sgRNA as an additional proof of a present or past virus replication. All positive results for the nasal wash samples collected

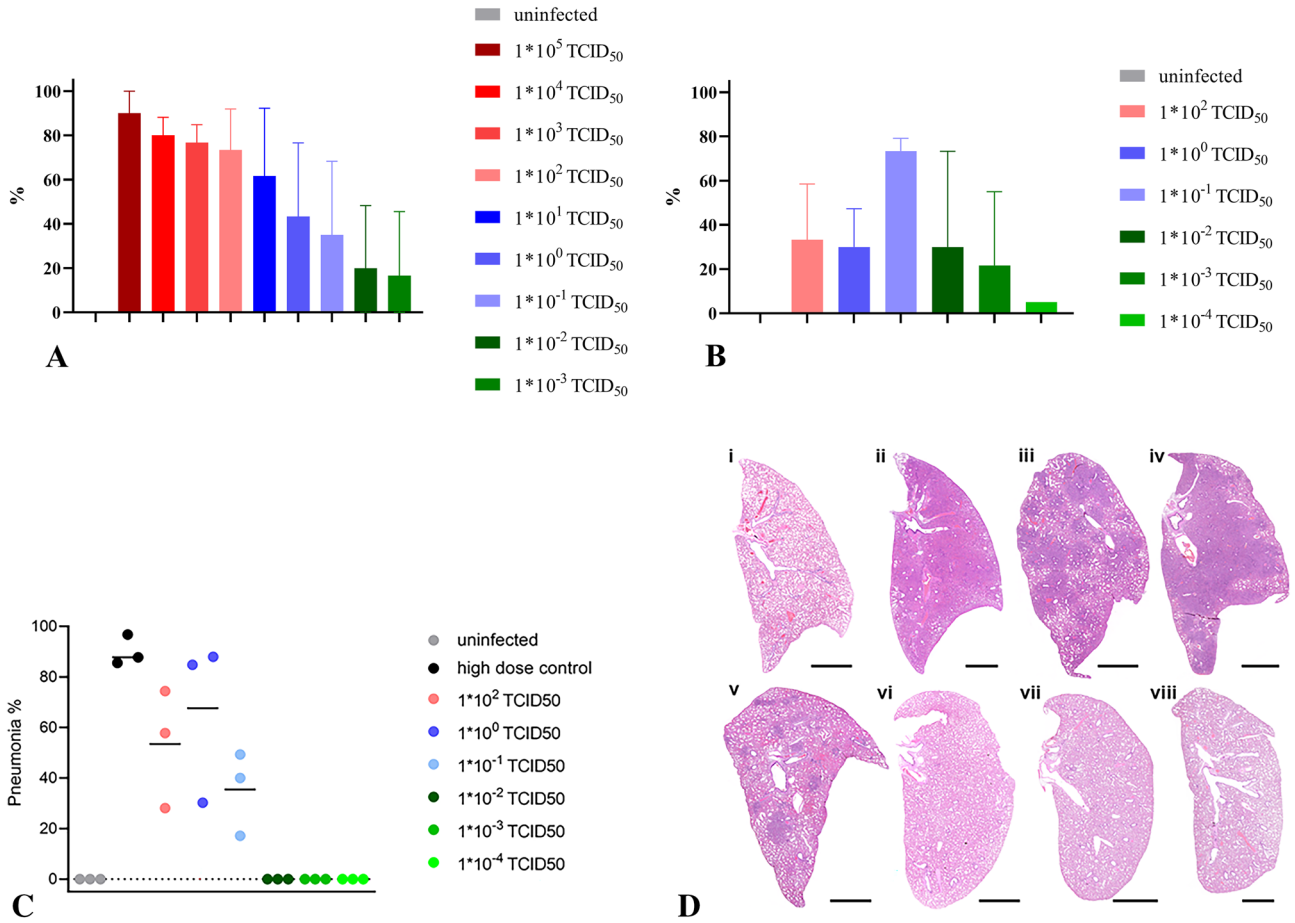

Figure 3. Levels of lung affection after challenge with different infection doses. (**A**) Macroscopically determined level of lesion-affection (%) of whole lung during autopsy at 7 dpi and (**B**) at 10 dpi displayed as the mean value and standard deviation for each group. (**C**, **D**) Histopathology of hamster lungs, 10 days after orotracheal SARS-CoV-2 infection. Pneumonia-associated consolidation (**C**) and representative overviews (**D**) of the entire left lung lobe of (i) uninfected control; (ii) high dose control; (iii) infected with $1 * 10^2$ $TCID_{50}$; (iv) infected with $1 * 10^0$ $TCID_{50}$; (v) infected with $1 * 10^{-1}$ $TCID_{50}$; (vi) infected with $1 * 10^{-2}$ $TCID_{50}$; (vii) infected with $1 * 10^{-3}$ $TCID_{50}$; (viii) infected with $1 * 10^{-4}$ $TCID_{50}$. (**B**)–(**D**) (n = 3).

at 2 and 4 dpi were confirmed by re-testing for sgRNA, with ct-values of about 3 points above those determined for the SARS-CoV-2-N-gene (Table S2). The peak of oral shedding of replication competent virus was observed between 3 and 5 dpi, at levels reaching up to 10^3 $TCID_{50}$/ml in the oral swab samples (Fig. 5B).

SARS-CoV-2 RNA levels detected in the nasal washes were generally 10- to 100- times higher than those determined from the oral swab samples. We were able to detect viral RNA at 2 and 4 dpi in nasal washes, even in the animals infected with the lowest dose of 10^{-4} $TCID_{50}$ (Fig. 6A). Significant differences were determined for the copy numbers detected in the different infection groups (Table S1). The peak of nasal shedding of replication competent virus was observed at 2 dpi at levels reaching up to 10^7 $TCID_{50}$/ml, while $1 * 10^{2.75}$ $TCID_{50}$ (equivalent to the estimated MID for humans), as well as sgRNA were detected in a sample collected from one animal infected with 10^{-3} $TCID_{50}$ (Fig. 6B and Table S2). The dose-dependent delay in onset of oral and nasal shedding is summarized in Fig. 7.

Replication competent SARS-CoV-2 virus in lungs after infection with $1 * 10^{-1}$ $TCID_{50}$, and in nasal conchae after infection with $1 * 10^{-3}$ $TCID_{50}$. Similar levels of viral RNA were detected in nasal conchae samples of all animals sacrificed at 7 dpi, independent of the inoculation dose, including the group infected with a dose of $1 * 10^{-3}$ $TCID_{50}$ (Fig. 8A), while at 10 dpi, viral RNA was only detected in the samples collected from the infection groups $1 * 10^2$ to $1 * 10^{-1}$ $TCID_{50}$ (Fig. 8B). Interestingly at 7 dpi, the highest levels of viral RNA were detected in trachea and lung samples collected in groups inoculated with the lowest infection dose of $1 * 10^{-3}$ $TCID_{50}$. At this time point, the highest virus titers were determined for the nasal conchae samples collected from animals infected with SARS-CoV-2 doses between 10^0 and 10^{-3} $TCID_{50}$ (Fig. 8C), which was confirmed by the detection of sgRNA (Table S2), while only nasal conchae samples from animals infected with 10^{-1} $TCID_{50}$ contained detectable levels of replication competent virus at 10 dpi (Fig. 8D). Statistically different levels of replication competent virus were detected in lung samples collected from animals inoculated with different infection doses (Table S1).

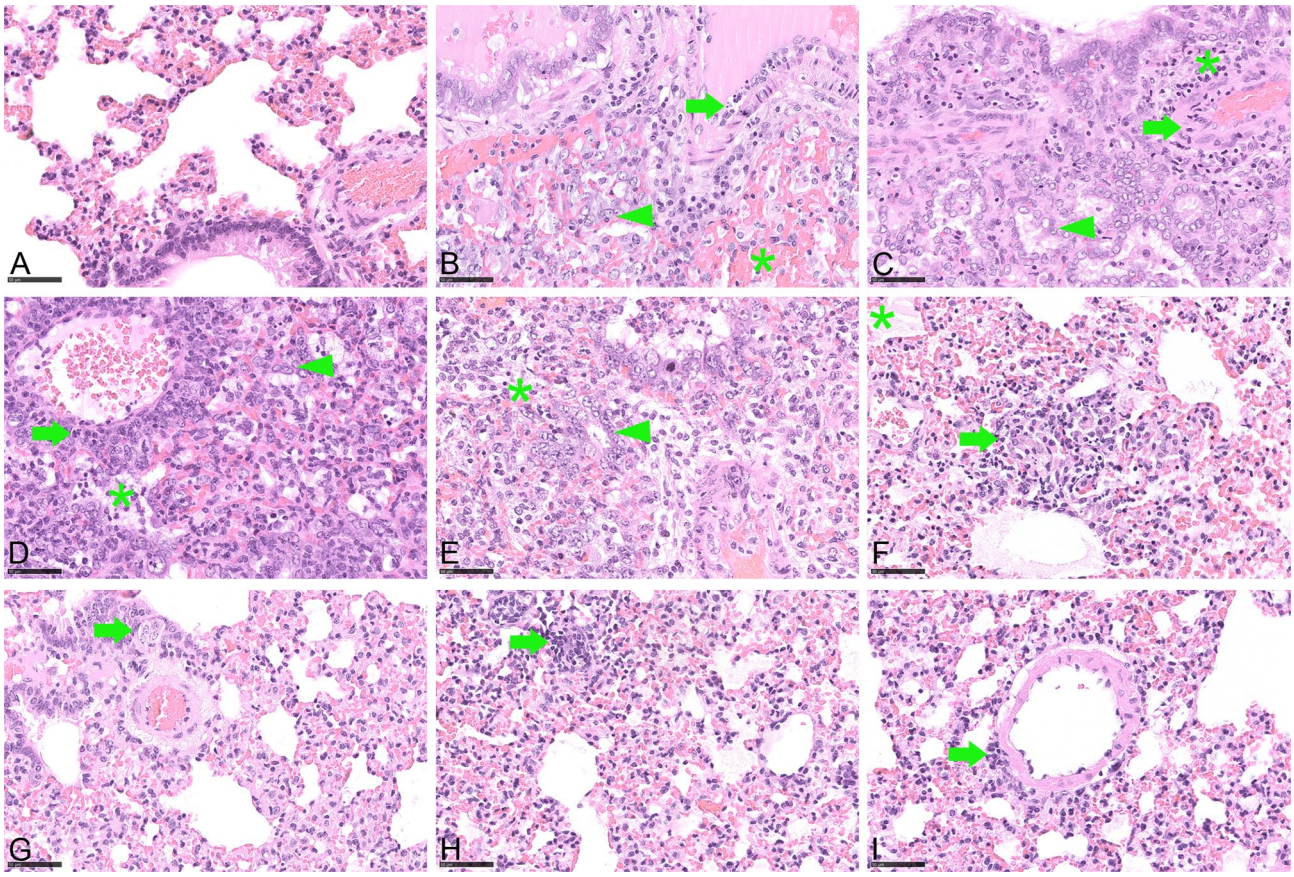

Figure 4. Detailed histopathology of hamster lungs, 10 days after orotracheal SARS-CoV-2 infection. Hematoxylin and eosin staining, bar 50 µm. (**A**) Uninfected control, no lung lesion, (**B**) after $1 * 10^{4.5}$ $TCID_{50}$ infection, showing vasculitis (arrow), type 2 pneumocyte hyperplasia and bronchialisation of alveoli (arrowhead), intra-alveolar erythrocytes (asterisk), (**C**) after $1 * 10^{2}$ $TCID_{50}$ infection, with vasculitis (arrow), type 2 pneumocyte hyperplasia and bronchialisation of alveoli (arrowhead) and perivascular infiltrates (asterisk), (**D**) after $1 * 10^{0}$ $TCID_{50}$ infection exhibiting perivascular (arrow) and alveolar (asterisk) infiltrates, type 2 pneumocyte hyperplasia and bronchialisation of alveoli (arrowhead), (**E**) after $1 * 10^{-1}$ $TCID_{50}$ infection, showing alveolar infiltrates (asterisk), type 2 pneumocyte hyperplasia and bronchialisation of alveoli (arrowhead), (**F**) after $1 * 10^{-2}$ $TCID_{50}$ infection, with focal alveolar infiltrates (arrow) and edema (asterisk), (**G**) after $1 * 10^{-3}$ $TCID_{50}$ infection, exhibiting focal hypertrophy/hyperplasia of bronchial epithelium (arrow), (**H**) after $1 * 10^{-4}$ $TCID_{50}$, with focal alveolar infiltrates (arrow), (**I**) after $1 * 10^{-4}$ $TCID_{50}$ showing focal perivascular infiltrates (arrow).

Sequence analysis of SARS-CoV-2 retrieved from animals infected with a high or a low dose. We exemplarily analysed SARS-CoV-2 whole-genome sequences retrieved from nasal conchae samples of two animals. Animal H310 (L5497) from a high-dose infection study ($1 * 10^{4.5}$ $TCID_{50}$) died at 6 dpi, whereas animal H318 (L5537) was infected with $1 * 10^{-1}$ $TCID_{50}$ and was autopsied 10 dpi. The sequence of the first sample is identical to the virus stock 2019_nCoV Muc-IMB-1 and shows only one single nucleotide variants (SNV), a transition in the M gene (C26877T) with 52% variant frequency (strand bias 51%) that was already detected as minor variant with 18% variant frequency in the virus stock. The sequence of the second animal is identical to the virus stock and shows only one transition in the ORF1a, nsp6 (T11639C) and no further SNVs. Both described changes are silent mutations. The genome sequences are available under ENA study accession number PRJEB51977.

Discussion

Today, Golden Syrian hamsters are the leading animal model in SARS-CoV-2 research, in particular for vaccine and drug efficacy studies[27–30], since they mirror the moderate disease phenotype of human patients with a complete recovery within 14 days[31]. When establishing this model, we initially used an infection dose of $1 * 10^{5}$ $TCID_{50}$, and found the orotracheal infection route to induce a more prominent weight loss and viral shedding, the latter exceeding those obtained after intranasal infection by at least a factor of 5. Therefore, this route was used for all subsequent studies. Since the intranasal route was used in almost all other published studies[27,28,30], and to the best of our knowledge no report of an orotracheal SARS-CoV-2 inoculation of hamsters has been published so far, a direct comparison between previously published experiments and our study is not feasible.

In our study, we were able to show that an infection dose of $1 * 10^{-1}$ $TCID_{50}$ was sufficient to induce a significant weight loss, oral and nasal shedding as well as accumulation of replication competent virus in the respiratory

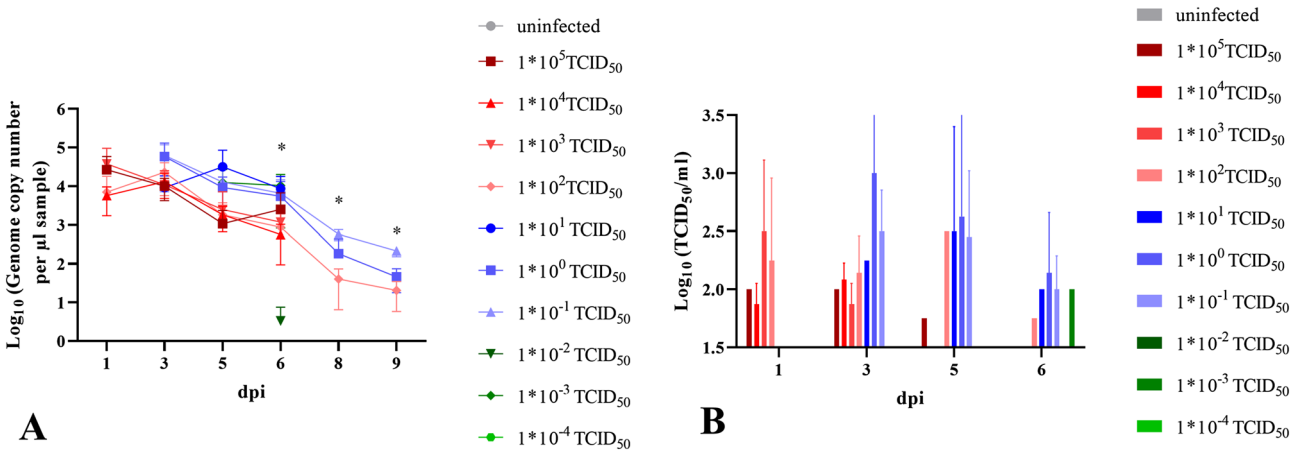

Figure 5. Viral shedding in oral swab samples. (**A**) Genome copy number (Log_{10}) of viral RNA and (**B**) replication competent virus (Log_{10} $TCID_{50}$/ml) detected in the oral swab samples of all hamsters. All groups were analysed, negative results are not shown. *p*-values are indicated for statistically significant differences in RNA levels. Details on statistical analysis are shown in Table S1. Colors match and represent results from the same hamsters as shown before and following.

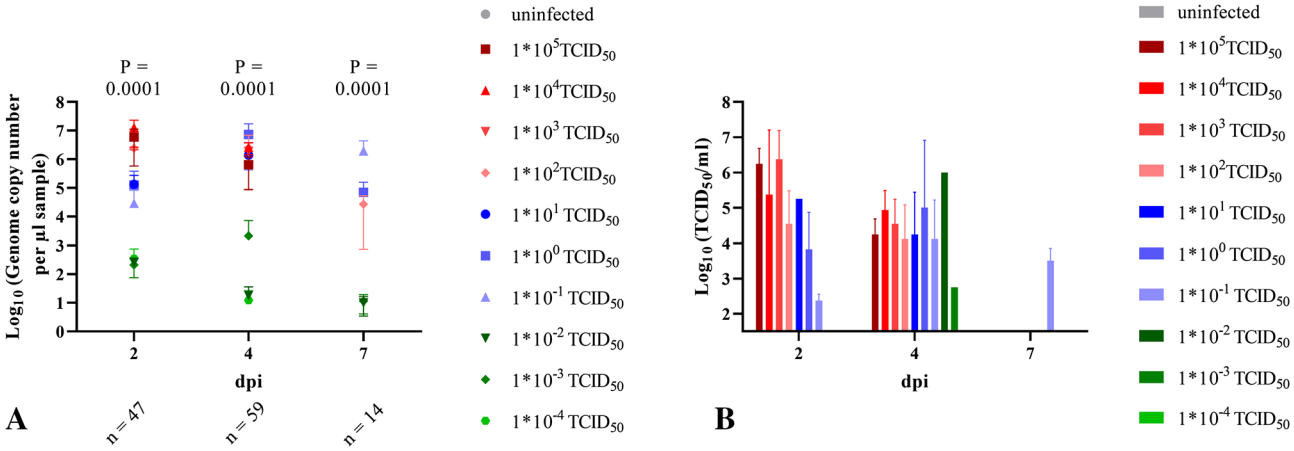

Figure 6. Viral shedding in nasal washes. (**A**) Genome copy number (Log_{10}) of SARS-CoV-2 RNA and (**B**) replication competent virus (Log_{10} $TCID_{50}$/ml) detected in the nasal wash samples of all hamsters 2, 4 and 7 dpi. All groups were analysed, negative results are not shown. Details on statistical analysis are shown in Table S1. Colors match and represent results from the same hamsters as shown before and following.

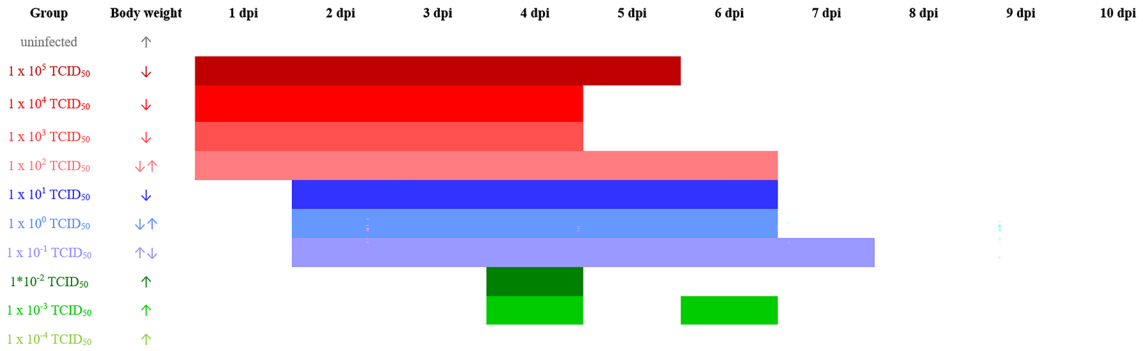

Figure 7. Time-dependent shedding of replication competent virus and change in body weight after infection with decreasing SARS-CoV-2 doses. Body weight development is shown by arrows; ↑ increasing from 1 to 7 or 10 dpi; ↓ decreasing from 1 to 7 or 10 dpi; ↓↑ decrease until 7 dpi followed by increase; ↑↓ increase until 4 dpi, followed by decrease until 10 dpi. Colors match and represent results from the same hamsters as shown before and following.

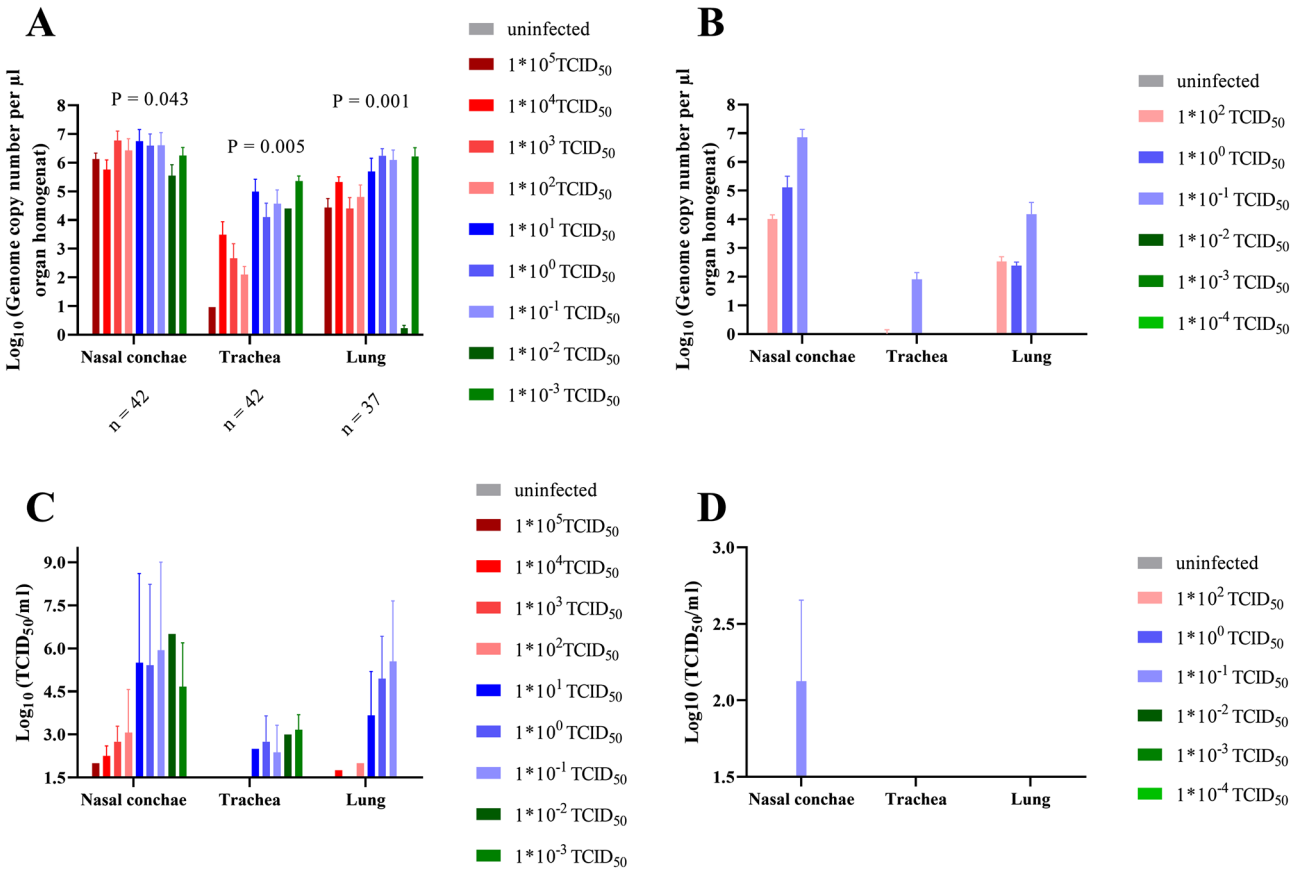

Figure 8. Genome copy number (Log_{10}) of SARS-CoV-2 RNA and replication competent virus (Log_{10} $TCID_{50}$/ml) detected in the respiratory tract. (**A**) Genome copy number (Log_{10}) of viral RNA and (**C**) replication competent virus (Log_{10} $TCID_{50}$/ml) detected in the respiratory tract samples at 7 dpi. (**B**) Genome copy number (Log_{10}) of viral RNA and (**D**) replication competent virus (Log_{10} $TCID_{50}$/ml) detected in the respiratory tract samples at 10 dpi. Statistically significant differences in RNA levels were determined at 7 dpi. Further details on statistical analysis are shown in Table S1. Colors match and represent results from the same hamsters as shown before.

tract, and SARS-CoV-2 related pneumonia. In this group, the onset of weight loss and lethargy were delayed by 3 days, presumably due to an initial virus replication at the inoculation site, before spreading throughout the respiratory tract. Infection doses of $1 * 10^{-2}$ $TCID_{50}$ or higher were sufficient to induce a dose-dependent seroconversion within 7 days, therefore the virus must have reached the lymphatic system within the first 2–3 days post infection. As no blood samples were available for time points before 7 dpi, a possible viremia within the first 3 days post infection could not be monitored. The estimated proportion of affected lung tissue also showed a clear correlation to the infection dose. Even after challenge with $1 * 10^{-3}$ $TCID_{50}$, we observed macroscopically visible lung affections, oral and nasal shedding as well as accumulation of replication competent virus in the nasal conchae and the trachea. We therefore define the MID for the ancestral virus variant used in this study for Golden Syrian hamsters upon orotracheal infection as $1 * 10^{-3}$ $TCID_{50}$. This result not only proves the exceptionally high susceptibility of Golden Syrian hamsters to a SARS-CoV-2 infection, but also indicates the low sensitivity of the Vero E6 virus titration assay with a detection limit of $1 * 10^{1.5}$ $TCID_{50}$, as compared to $1 * 10^{-3}$ $TCID_{50}$ in the Golden Syrian hamster model. In another Golden Syrian hamster susceptibility study published by Rosenke and co-workers[32] using intranasal infection doses between $1 * 10^{3}$ and $1 * 10^{0}$ $TCID_{50}$, a dose of 5 $TCID_{50}$ was postulated as MID. The data obtained for the lower dose group resembles what we observed for the group inoculated with $1 * 10^{-2}$ $TCID_{50}$, which may be due to the increased efficiency of the orotracheal route. Moreover, since data were only collected until 5 dpi, a delayed onset of virus shedding and virus propagation in the respiratory tract after challenge with very low doses would have remained unnoticed.

We propose an optimal SARS-CoV-2 infection dose for drug or vaccine efficacy studies in Golden Syrian hamsters of 10^2 $TCID_{50}$ for the ancestral virus variant used in this study, as this is sufficient to induce a reproducible (as confirmed by three independent experiments) weight loss, macroscopically visible lung affection, pneumonia, shedding of replication competent virus from 1 dpi, and the presence of high levels of replication competent virus in the respiratory tract on day 7 post infection, which will therefore allow a quantification of therapeutic effects. Infection doses of 10^5 $TCID_{50}$ that are generally used in Golden Syrian hamsters[5,7,33,34] may be too high to allow a disease progression at least partly resembling the distinctly slower processes in humans after a natural infection[4].

Replication competent virus as well as SARS-CoV-2 sgRNA were detectable at dose dependent levels in nasal washes of all groups until 4 dpi except the group infected with $1 * 10^{-4}$ $TCID_{50}$. Thus, by this time, the virus must have already disseminated from the trachea and lung (inoculation site) to the upper respiratory tract, which may have occurred either via mucus transport from the lower respiratory tract, or via the bloodstream. Since we did not determine seroconversion in the animals receiving an infection dose of $1 * 10^{-2}$ $TCID_{50}$ or lower, virus dissemination via active mucus transport seems most plausible. The positive sgRNA results also indicate a past active viral replication in the nasal epithelium, as sgRNAs are transcribed only in infected cells[18]. However, positive sgRNA results cannot be interpreted as an equivalent to the detection of replication competent virus by $TCID_{50}$[23].

To allow a first insight whether the exposition to immune reactions in an animal inoculated with a low dose may stimulate the formation of gene mutations, we analysed the SARS-CoV-2 sequences retrieved from nasal conchae samples from one animal each infected with a high dose and a low dose, and found no indication for such an effect.

The confirmation of SARS-CoV-2 infections in animals infected with $1 * 10^{-1}$ $TCID_{50}$ or higher by LFD confirms the suitability of these assays for the screening of hamster swab samples, which may be relevant in households with COVID-19 patients where Golden Syrian hamsters are kept as pets. Upon natural infection with a low dose, these animals will most probably not develop clinical signs, but will shed replication competent virus for at least 6 days at levels possibly exceeding the estimated human MID of $1 * 10^{2}$ $TCID_{50}$, thus allowing a zoonotic infection cycle between humans and Syrian Golden hamsters, as it has been observed very recently in Hong Kong[15]. However, any positive private LFD result should be confirmed by an official test performed by a veterinarian.

Our data demonstrate the exceptionally high susceptibility of Golden Syrian hamsters to an infection with a German SARS-CoV-2 isolate obtained during an outbreak in Munich in January 2020[18]. Although we detected the presence of replication competent SARS-CoV-2 virus at high titers in swab samples, nasal wash fluid and nasal turbinates, hamsters do not seem to play a major role in the dynamics of the pandemic itself. We attribute this to the low respiratory volume of these animals, resulting in a lower level of virus aerosolization in comparison to larger animal species or humans. The titers determined in the nasal wash samples of animals challenged with doses between 10^{5} and 10^{-2} $TCID_{50}$ reached comparable levels of 10^{5} to 10^{6} $TCID_{50}$/ml between 2 and 4 dpi. Earlier studies have shown that these levels are sufficient to induce intraspecies transmission between hamsters, even by aerosol transmission without direct contact between the animals[5]. Other groups reported an almost identical disease progression and virus shedding pattern for VOCs Alpha, Beta, and Delta as for the ancestral virus in hamsters[10,11], rendering the titration experiments with these VOCs dispensable. Meanwhile, a low pathogenicity combined with high up to 100-fold increased viral loads in the upper respiratory tract were reported for hamsters infected with the Omicron variant[12,35]. Therefore, an Omicron titration study in hamsters similar to what we describe here for the ancestral virus may be rewarding.

In summary, we determined the extremely high susceptibility of Golden Syrian hamsters to a SARS-CoV-2 infection, and defined the MID as $1 * 10^{-3}$ $TCID_{50}$. A very close monitoring of pet Golden Syrian hamsters that are kept in households with COVID-19 patients is therefore strongly recommended, for instance by using rapid tests. COVID-19 patients should strictly avoid any direct or indirect contact to their pet hamsters. The optimal infection dose for drug efficacy studies was determined as $1 * 10^{2}$ $TCID_{50}$. These conclusions not only apply to Golden Syrian hamsters, but likely also to Chinese hamsters (*Cricetulus griseus*) and Roborovski Dwarf hamsters (*Phodopus roborovskii*), since these two species have been shown to also be highly susceptible[8,9].

Data availability

All data needed to evaluate the conclusions in the paper are present in the paper and/or the Supporting Information. The genome sequences are available under ENA study accession number PRJEB51977 (https://www.ebi.ac.uk/ena/browser/view/PRJEB51977).

Received: 28 May 2022; Accepted: 25 August 2022
Published online: 05 September 2022

References

1. Cheng, C. *et al.* The incubation period of COVID-19: a global meta-analysis of 53 studies and a Chinese observation study of 11 545 patients. *Infect. Dis. Poverty* **10**, 119. https://doi.org/10.1186/s40249-021-00901-9 (2021).
2. Elias, C., Sekri, A., Leblanc, P., Cucherat, M. & Vanhems, P. The incubation period of COVID-19: a meta-analysis. *Int. J. Infect. Dis.* **104**, 708–710. https://doi.org/10.1016/j.ijid.2021.01.069 (2021).
3. Basu, S. Computational characterization of inhaled droplet transport to the nasopharynx. *Sci. Rep.* **11**, 6652. https://doi.org/10.1038/s41598-021-85765-7 (2021).
4. Karimzadeh, S., Bhopal, R. & Nguyen Tien, H. Review of infective dose, routes of transmission and outcome of COVID-19 caused by the SARS-COV-2: comparison with other respiratory viruses- CORRIGENDUM. *Epidemiol. Infect.* **149**, e116. https://doi.org/10.1017/S0950268821001084 (2021).
5. Chan, J. F. *et al.* Simulation of the clinical and pathological manifestations of coronavirus disease 2019 (COVID-19) in a golden Syrian hamster model: implications for disease pathogenesis and transmissibility. *Clin. Infect. Dis.* **71**, 2428–2446. https://doi.org/10.1093/cid/ciaa325 (2020).
6. Sia, S. F. *et al.* Pathogenesis and transmission of SARS-CoV-2 in golden hamsters. *Nature* **583**, 834–838. https://doi.org/10.1038/s41586-020-2342-5 (2020).
7. Dowall, S. *et al.* Development of a hamster natural transmission model of SARS-CoV-2 infection. *Viruses* **13**, 2251 (2021).
8. Bertzbach, L. D. *et al.* SARS-CoV-2 infection of Chinese hamsters (Cricetulus griseus) reproduces COVID-19 pneumonia in a well-established small animal model. *Transbound. Emerg. Dis.* **68**, 1075–1079. https://doi.org/10.1111/tbed.13837 (2021).
9. Trimpert, J. *et al.* The roborovski dwarf hamster is a highly susceptible model for a rapid and fatal course of SARS-CoV-2 infection. *Cell Rep.* **33**, 108488. https://doi.org/10.1016/j.celrep.2020.108488 (2020).

10. O'Donnell, K. L. *et al.* Pathogenic and transcriptomic differences of emerging SARS-CoV-2 variants in the Syrian golden hamster model. *EBioMedicine* **73**, 103675. https://doi.org/10.1016/j.ebiom.2021.103675 (2021).
11. Mohandas, S. *et al.* SARS-CoV-2 delta variant pathogenesis and host response in Syrian hamsters. *Viruses* https://doi.org/10.3390/v13091773 (2021).
12. Abdelnabi, R. *et al.* The omicron (B.1.1.529) SARS-CoV-2 variant of concern does not readily infect Syrian hamsters. *Antiviral Res.* **198**, 105253. https://doi.org/10.1016/j.antiviral.2022.105253 (2022).
13. McMahan, K. *et al.* Reduced pathogenicity of the SARS-CoV-2 omicron variant in hamsters. *Med (N Y)* **3**, 262-268.e264. https://doi.org/10.1016/j.medj.2022.03.004 (2022).
14. Mohandas, S. *et al.* Pathogenicity of SARS-CoV-2 Omicron (R346K) variant in Syrian hamsters and its cross-neutralization with different variants of concern. *EBioMedicine* **79**, 103997. https://doi.org/10.1016/j.ebiom.2022.103997 (2022).
15. Yen, H. L. *et al.* Transmission of SARS-CoV-2 delta variant (AY.127) from pet hamsters to humans, leading to onward human-to-human transmission: a case study. *Lancet* **399**, 1070–1078. https://doi.org/10.1016/S0140-6736(22)00326-9 (2022).
16. Kok, K. H. *et al.* Co-circulation of two SARS-CoV-2 variant strains within imported pet hamsters in Hong Kong. *Emerg. Microbes Infect.* **11**, 689–698. https://doi.org/10.1080/22221751.2022.2040922 (2022).
17. Haagmans, B. L. & Koopmans, M. P. G. Spreading of SARS-CoV-2 from hamsters to humans. *Lancet* **399**, 1027–1028. https://doi.org/10.1016/S0140-6736(22)00423-8 (2022).
18. Wolfel, R. *et al.* Virological assessment of hospitalized patients with COVID-2019. *Nature* **581**, 465–469. https://doi.org/10.1038/s41586-020-2196-x (2020).
19. Wylezich, C., Papa, A., Beer, M. & Hoper, D. A versatile sample processing workflow for metagenomic pathogen detection. *Sci. Rep.* **8**, 13108. https://doi.org/10.1038/s41598-018-31496-1 (2018).
20. Atkinson, G. F. *The Spearman-Karber Method of Estimating 50% Endpoints* (Cornell University, 1961).
21. Schlottau, K. *et al.* SARS-CoV-2 in fruit bats, ferrets, pigs, and chickens: an experimental transmission study. *Lancet Microbe* **1**, e218–e225. https://doi.org/10.1016/S2666-5247(20)30089-6 (2020).
22. Corman, V. M. *et al.* Detection of novel coronavirus (2019-nCoV) by real-time RT-PCR. *Eurosurveillance* https://doi.org/10.2807/1560-7917.ES.2020.25.3.2000045 (2019).
23. Alexandersen, S., Chamings, A. & Bhatta, T. R. SARS-CoV-2 genomic and subgenomic RNAs in diagnostic samples are not an indicator of active replication. *Nat. Commun.* **11**, 6059. https://doi.org/10.1038/s41467-020-19883-7 (2020).
24. Hoffmann, D. *et al.* CVnCoV and CV2CoV protect human ACE2 transgenic mice from ancestral B BavPat1 and emerging B.1.351 SARS-CoV-2. *Nat. Commun.* **12**, 4048. https://doi.org/10.1038/s41467-021-24339-7 (2021).
25. Wernike, K. *et al.* Multi-species ELISA for the detection of antibodies against SARS-CoV-2 in animals. *Transbound. Emerg. Dis.* **68**, 1779–1785. https://doi.org/10.1111/tbed.13926 (2021).
26. Meyerholz, D. K. & Beck, A. P. Principles and approaches for reproducible scoring of tissue stains in research. *Lab. Invest.* **98**, 844–855. https://doi.org/10.1038/s41374-018-0057-0 (2018).
27. Chiba, S. *et al.* Co-administration of favipiravir and the remdesivir metabolite GS-441524 effectively reduces SARS-CoV-2 replication in the lungs of the Syrian hamster model. *mBio* **13**, e0304421. https://doi.org/10.1128/mbio.03044-21 (2022).
28. Taylor, R. *et al.* Activity of galidesivir in a hamster model of SARS-CoV-2. *Viruses* https://doi.org/10.3390/v14010008 (2021).
29. Meseda, C. A. *et al.* MVA vector expression of SARS-CoV-2 spike protein and protection of adult Syrian hamsters against SARS-CoV-2 challenge. *NPJ Vaccines* **6**, 145. https://doi.org/10.1038/s41541-021-00410-8 (2021).
30. Yadav, P. D. *et al.* ZRC3308 monoclonal antibody cocktail shows protective efficacy in Syrian hamsters against SARS-CoV-2 infection. *Viruses* **13**, 2424 (2021).
31. Gruber, A. D., Firsching, T. C., Trimpert, J. & Dietert, K. Hamster models of COVID-19 pneumonia reviewed: how human can they be?. *Vet. Pathol.* https://doi.org/10.1177/03009858211057197 (2021).
32. Rosenke, K. *et al.* Defining the Syrian hamster as a highly susceptible preclinical model for SARS-CoV-2 infection. *Emerg. Microbes Infect.* **9**, 2673–2684. https://doi.org/10.1080/22221751.2020.1858177 (2020).
33. Johnson, S. *et al.* Oral vaccination protects against severe acute respiratory syndrome coronavirus 2 in a Syrian hamster challenge model. *J. Infect. Dis.* **225**, 34–41. https://doi.org/10.1093/infdis/jiab561 (2022).
34. Francis, M. E. *et al.* SARS-CoV-2 infection in the Syrian hamster model causes inflammation as well as type I interferon dysregulation in both respiratory and non-respiratory tissues including the heart and kidney. *PLoS Pathog.* **17**, e1009705. https://doi.org/10.1371/journal.ppat.1009705 (2021).
35. McMahan, K. *et al.* Reduced pathogenicity of the SARS-CoV-2 omicron variant in Hamsters. bioRxiv, 2022.2001.2002.474743. https://doi.org/10.1101/2022.01.02.474743 (2022).

Acknowledgements

Daniel Balkema, Weda Hoffmann, Julia Neumeister, Silvia Schuparis, Emilie Stutz and Patrick Zitzow are thanked for their excellent technical assistance. Doreen Fiedler, Steffen Kiepert, Frank Klipp, Christian Lipinski and Harald Manthei are thanked for their support in the animal experiments.

Author contributions

Conceptualization: A.B.-B., C.B.; Methodology: A.B.-B., C.B., M.K.; Formal analysis: C.B., B.-P.M., B.S., A.B.; Investigation: A.B.-B., C.B., B.-P.M., A.B., S.W., C.W.; Visualization: C.B., B.-P.M., A.B.; Supervision: A.B.-B., D.H.; Writing—original draft: A.B.-B., C.B., B.-P.M.; Writing—review and editing: T.C.M., M.H.G., D.H., D.G.; Resources: D.G., M.H.G., T.C.M. All authors have read and agreed to the published version of the manuscript.

Funding

Open Access funding enabled and organized by Projekt DEAL. Funding was provided by Max-Planck-Gesellschaft, Max-Planck-Förderstiftung and FLI-internal funds. The funders had no role in study design, data collection and analysis, decision to publish or preparation of the manuscript.

Competing interests

The authors declare no competing interests.

Additional information

Supplementary Information The online version contains supplementary material available at https://doi.org/10.1038/s41598-022-19222-4.

Correspondence and requests for materials should be addressed to A.B.-B.